analytical chemistry

Article

pubs.acs.org/ac

Inertia-Enhanced Pinched Flow Fractionation

Xinyu Lu and Xiangchun Xuan*

Department of Mechanical Engineering, Clemson University, Clemson, South Carolina 29634-0921, United States

ABSTRACT: Separating target particles or cells from a heterogeneous mixture is often critical to many chemical and biomedical applications. Pinched flow fractionation (PFF) is a microfluidic technique that utilizes the laminar flow profile to continuously separate particles by size. We demonstrate that the flow-induced inertial lift force in microchannels can be exploited to significantly increase the particle displacement in PFF due to its strong size dependence. This inertia-enhanced PFF (iPFF) technique can offer at least one-order-of-magnitude higher particle throughput than PFF does at the same sheath flow rate. Moreover, it is able to work effectively in a large range of Reynolds number that spans more than 1 order of magnitude in the current study. In addition, iPFF is found to work most effectively in a rectangular microchannel with a width-to-height aspect ratio of around 2.

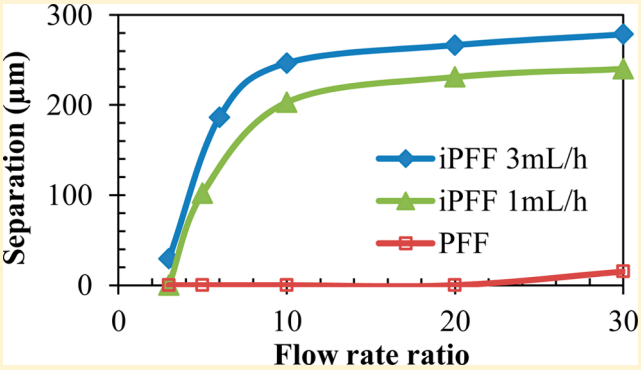

Separating target particles (either synthetic or biological) from a heterogeneous mixture is often critical to many chemical and biomedical applications.[1,2] To date, a variety of microfluidic techniques have been developed to separate various types of particles based on either intrinsic properties (e.g., size, density, and shape) or external labeling (e.g., fluorescent and magnetic tagging).[3−8] Pinched flow fractionation (PFF) is one such technique that utilizes the laminar flow profile in microchannels to continuously separate particles by size.[9−12] In a PFF microdevice, particles of different sizes must first be focused against one sidewall of a microchannel via a strong sheath flow that can be pressure-[9−12] and electric field-driven.[13,14] This alignment causes the centers of particles to locate at size-dependent streamlines in the short pinched segment. The separation distance between particles is then amplified in the abruptly broadened segment due to the hydrodynamic spreading. For a theoretically 100% separation via PFF, the maximum allowed width of the sheath flow-focused particulate solution, $w_{p,max}$, in a microchannel with an infinitely wide broadened segment must fulfill the following condition,[9,15]

$$w_{p,max} = r_{p1} + r_{p2} \quad (1)$$

where r_{p1} and r_{p2} are the radii of the two types of particles (each is assumed of a uniform size) to be separated. This value of $w_{p,max}$ corresponds to the limiting circumstance at which the center position of the aligned larger particles becomes identical to that of the smaller particles most distant from the sidewall.

Since its first demonstration by Yamada et al. in 2004,[9] PFF has been continuously improved over the past decade in primarily two aspects: one is to increase the particle displacement and the other is to reduce the particle dispersion. For the former approach, the displacement between particles of dissimilar sizes can be increased inside the pinched segment by introducing an additional force field perpendicular to the flow such as gravity,[16] optical force,[17] and electrical lift.[18] Alternatively, the particle displacement in PFF can be augmented within the broadened segment through the introduction of a snakelike structure[19] or the arrangement of multiple asymmetric branches.[20−24] It can also been increased via the use of a polymer sheath fluid to viscoelastically tune the hydrodynamic spreading in the broadened segment.[25] For the second approach, the particle dispersion in PFF[26] can be dramatically reduced by adding a tilted sidewall as well as vertical focusing channels to the pinched segment to precisely align particles of different sizes.[27] In addition, the particle separation in PFF has been numerically investigated using, for example, boundary-integral method[28,29] and lattice Boltzmann method,[30,31] which provides guidance for the optimal design of future PFF microdevices.

We propose to exploit the flow-induced inertial lift force in an elongated pinched segment to increase the particle displacement in PFF for an enhanced separation. The inertial lift force intrinsic to particles in confined channel flows has been extensively studied since the seminal work from Segre and Silberberg[32] more than a half century ago.[33−38] Particularly inspired by the pioneering work from Di Carlo et al.,[39] the inertial particle migration has been increasingly used in microfluidic devices to manipulate particles in a high-throughput manner over the past decade or so.[40−42] This cross-stream particle motion, either alone in straight micro-channels[43−47] or combined with Dean flow in curved[48−52] and

Received: February 25, 2015
Accepted: April 3, 2015
Published: April 3, 2015

 © 2015 American Chemical Society

DOI: 10.1021/acs.analchem.5b00752
Anal. Chem. 2015, 87, 4560−4565

converging-diverging microchannels,[53−55] has been demonstrated to separate particles based on the difference in their equilibrium positions. Such a size-dependent migration is utilized in this work to increase the particle deflection and hence the separation distance between particles in PFF. This inertia-enhanced PFF (iPFF) technique will be experimentally demonstrated and investigated in terms of three defined dimensionless numbers, that is, Reynolds number, sheath-fluid to particle-mixture flow rate ratio, and channel aspect ratio.

EXPERIMENTAL SECTION

The standard soft lithography method was used to fabricate the microchannels with polydimethylsiloxane (PDMS). The detailed procedure can be referred to Lu et al.[56] Three depths of channels are used in our experiments, which are 15, 25, and 40 μm, respectively. As shown in Figure 1, each depth of microchannel has a 2 cm long main branch and two 4 mm long side branches with a uniform width of 50 μm. At the end of the main branch, a 900 μm wide expansion with a 2 mm length is designed to enhance the particle separation, which also serves as the viewing window as highlighted by the dashed-box in Figure 1. Polystyrene spheres (Thermo Scientific) with a diameter of 3.1 and 9.9 μm, respectively, were mixed in an approximately 2:1 number density ratio and resuspended in pure water (Fisher Scientific) to a concentration of about 10^7 particles per milliliter. To reduce the influences of particle adhesions to microchannel walls and particle aggregations, a small amount of Tween 20 (0.5% in volume ratio, Fisher Scientific) was added to the particle suspension. The sheath fluid (i.e., pure water) and particle mixture were pumped through the side branches of the microchannel by two independent syringe pumps (NE-300 from New Era Pump Systems for the sheath fluid and KDS-100 from KD Scientific for the particle mixture). The separation of particles was visualized at the channel expansion region through an inverted microscope (Nikon Eclipse TE2000U, Nikon Instruments) with a CCD camera (Nikon DS-Qi1Mc). The recorded digital images were postprocessed using the Nikon imaging software (NIS-Elements AR 3.22). Particle streak images were obtained by superimposing a sequence of typically 450 images.

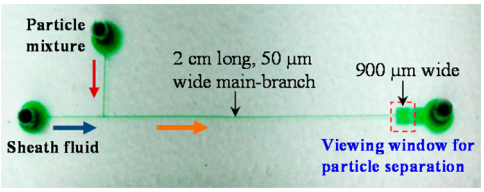

Figure 1. Top-view picture of the microchannel (filled with green food dye for clarity) used in experiments on particle separation via iPFF. The block arrows indicate the flow directions in the side branches and main branch of the microchannel. The particle separation is viewed at the 900 μm wide expansion region at the end of the 2 cm long, 50 μm wide main branch.

THEORETICAL

Dimensionless Numbers. The inertial migration of particles in confined channel flows is dependent on Reynolds number, Re, which is defined as the ratio of the inertial force to the viscous force,

$$\mathrm{Re} = \frac{\rho V D_h}{\eta_0} = \frac{2\rho Q}{\eta_0 (w + h)} \tag{2}$$

where V is the average fluid velocity in the main branch of the T-shaped microchannel in Figure 1, $D_h = 2wh/(w + h)$ is the hydraulic diameter with w and h being the width and height of the main branch, and Q is the volumetric flow rate through the main branch. The flow rate ratio between the sheath fluid, Q_{sheath}, and the particle mixture, $Q_{particle}$, in the two side branches, α,

$$\alpha = \frac{Q_{sheath}}{Q_{particle}} \tag{3}$$

is the second dimensionless number involved in this work. It measures the sheath flow focusing performance in the main branch and affects the particle dispersion at the channel expansion. Note that the definitions of Re in eq 2 is based on the total flow rate in the main branch of the microchannel, that is, $Q = Q_{sheath} + Q_{particle}$. The third dimensionless number to be used in this work is the channel aspect ratio, AR,

$$\mathrm{AR} = w/h \tag{4}$$

which has been demonstrated to affect both the number and the location of equilibrium positions for particle motions in rectangular microchannel flows.[40−42,57,58] It will be used to study the influence of channel depth on particle separation via iPFF.

Mechanism of iPFF. Similar to the traditional PFF,[9] the particle mixture in our proposed iPFF is first focused by a sheath fluid to a thin layer near one sidewall of the microchannel at the T-junction in Figure 1. The flow-induced inertial lift force, $\mathbf{F}_{iL}$, in the elongated rectangular main branch then takes effects to push particles away from the sidewall as schematically shown in Figure 2,[37]

$$\mathbf{F}_{iL} = C_L \rho r_p^4 \dot{\gamma}^2 \tag{5}$$

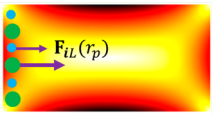

Figure 2. Schematic illustrating the mechanism of the proposed particle separation via iPFF. The background color (the darker the larger magnitude) shows the contour of the fluid shear rate, $\dot{\gamma}$, over the channel cross-section, which was obtained from a 3D flow simulation (COMSOL) in a straight 50 μm (w) × 25 μm (h) microchannel (i.e., AR = 2.0). The symbol $\mathbf{F}_{iL}$ represents the inertial lift force experienced by a suspended particle in a confined geometry, which is a strong function of particle size, r_p, as given by eq 5.

where the dimensionless lift coefficient C_L is a function of Re, AR, and particle position, ρ is the density of the suspending fluid, r_p is the particle radius, and $\dot{\gamma}$ is the fluid shear rate. Since $\mathbf{F}_{iL}$ is a strong function of particle size, the lateral displacement between particles can be significantly increased yielding an enhanced separation via iPFF. Moreover, the mixture of particles need not be tightly focused at the T-junction, that is, the width of the particulate solution in the main branch can be larger than the maximum allowed width, that is, $w_{p,max}$ in eq 1, as we will demonstrate in Results and Discussion. As a result, the particle throughput in the proposed iPFF will be greater than that in the traditional PFF if the sheath flow rate is fixed.

DOI: 10.1021/acs.analchem.5b00752
Anal. Chem. 2015, 87, 4560−4565

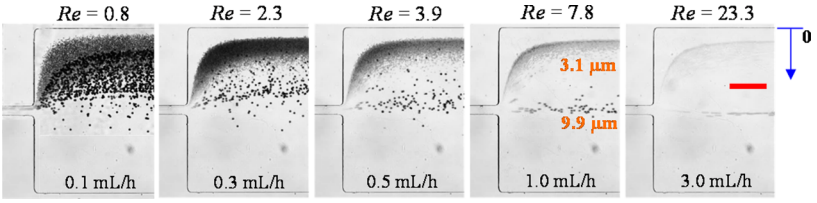

Figure 3. Superimposed images at the expansion of the microchannel illustrating the effect of fluid inertia, Re (highlighted on top of the images), on the continuous separation of 3.1 and 9.9 μm diameter particles via iPFF in a 25 μm deep microchannel (i.e., AR = 2.0) at various sheath flow rates (labeled on the images). The flow rate ratio between sheath fluid and particle mixture is maintained at α = 20. The vertical arrow on the right-most image indicates the reference point to which the particle stream positions in Figure 4 were measured. The scale bar represents 200 μm. The flow direction is from left to right in all images.

In the literature, the inertial lift force, $\mathbf{F}_{iL}$, on a suspended particle in confined flows has been often understood as the addition of two primary components.[40−42] The first is the wall-induced lift that deflects particles away from the channel walls. The second is the shear gradient-induced lift that directs particles toward the regions of high shear rate, which, as seen from the contour of fluid shear rate, $\dot{\gamma}$, in Figure 2 (the background color, the darker the higher magnitude), occur near the channel walls. The combined action of these two lift components leads to the formation of four equilibrium particle positions centered at the faces of (nearly) square microchannels, which are each approximately at 0.6 of the normal distance from the channel center to the channel wall.[59] However, the number of equilibrium positions is reported to reduce to preferentially two centered at the wider faces of rectangular microchannels. This variation has been recently attributed to the rotation-induced lift force[57] that plays an important role for near-wall particles.[60] Therefore, the larger particles are expected to migrate quickly toward the center position of the horizontal plane in a rectangular microchannel with a high aspect ratio (e.g., AR = 50 μm/25 μm = 2.0 in Figure 2), leaving behind the smaller particles due to the strong dependence of $\mathbf{F}_{iL}$ on particle size in eq 5.

RESULTS AND DISCUSSION

Effect of Fluid Inertia (Re). The superimposed images in Figure 3 compare the continuous separation of 3.1 and 9.9 μm diameter particles via iPFF in a 25 μm-deep microchannel (i.e., AR = 2.0) at different Re. The shear flow rate, Q_{sheath}, is varied from 0.1 to 5 mL/h, while the flow rate ratio between sheath fluid and particle mixture is maintained at α = 20. Note that the values of Re shown in Figure 3 were all calculated using the total flow rate in the main branch of the channel, that is, $Q = (1 + 1/\alpha)Q_{sheath} = 1.05Q_{sheath}$. We did a 3D numerical simulation of the flow field in the microchannel for α = 20 (COMSOL) and found that the particle solution is focused to a fluid layer of w_p = 6.3 μm wide in the main branch. This value is slightly less than the maximum allowed width of the focused particle solution, that is, $w_{p,max} = (3.1 + 9.9)/2 = 6.5$ μm in eq 1. However, a complete separation of 3.1 and 9.9 μm diameter particles is still unachievable in the current microchannel (Figure 1) if the inertial lift force does not play a role. This is because the theoretically predicted particle separation distance (which is from edge to edge), SD_{PFF}, for the traditional PFF,

$$SD_{PFF} = (r_{p1} + r_{p2} - w_p)\frac{w_{expansion}}{w_{channel}} - (r_{p1} + r_{p2}) \quad (6)$$

is less than zero for w_p = 6.3 μm in our microchannel, where the widths of the expansion and main branch are $w_{expansion}$ = 900 μm and $w_{channel}$ = 50 μm, respectively. Note that the first term on the right hand side of eq 6 gives only the particle center-to-center distance in the channel expansion. This equation is obtained with the assumption that particles strictly follow streamlines, which, as explained in previous numerical studies,[28−31] may cause inaccuracy due to the corner effect.

The above analysis is supported by the observation in Figure 3 at the smallest Re = 0.8, where the inertial effects are still weak even in the long main branch, and hence, the two particle zones are significantly overlapped in the expansion region as expected. With the increase of Re, 9.9 μm particles are apparently pushed away from the sidewall by the inertial lift, $\mathbf{F}_{iL}$, and directed toward the channel centerline. Moreover, the dispersion of these particles seems to decrease with Re, which may be due to the fact that their equilibrium positions are centered at the faces of the top and bottom channel walls.[57−59] In contrast, the deflection of 3.1 μm particles remains nearly unaffected by Re due to the strong size dependence of $\mathbf{F}_{iL}$ in eq 5. As such, a clear separation gap is formed between the two types of particles at Re > 3.9, as demonstrated in Figure 3. It, however, does not vary significantly when Re > 7.8 (corresponding to Q_{sheath} = 1 mL/h) because 9.9 μm particles have almost attained their equilibrium position along the channel centerline. With reference to the analysis of Zhang et al.,[61] the centrifugal force due to the inertia of particle at the corner of the expansion was estimated to be small because the particle density (1.05 g/cm^3) closely matches that of the suspending fluid (1.0 g/cm^3). Therefore, its contribution to the particle deflection and separation in the expansion region, where Re is significantly lower than that in the main branch, should be minimal if not negligible. We did not test Re > 38.9 (corresponding to Q_{sheath} > 5 mL/h) due to the limited resolution of the camera. It is also important to note that additional equilibrium positions near the two sidewalls have been recently reported to occur for very high Re (around 200) in a rectangular microchannel with AR = 2.0,[58] which can cause a decreased particle separation via iPFF.

A quantitative analysis of the exiting positions of the two particle streams at the channel expansion versus Re is shown in Figure 4. The data (symbols) were measured directly from the particle images in Figure 3, where the top sidewall of the channel expansion was used as the reference point (see the vertical arrow on the right-most image) and the center of the particle traces with the lowest intensity (note the lower intensity, the darker in a gray scale image) was used as the measuring point. Error bars were included for both particles in Figure 4 to cover the span of each particle stream. The center position of the 3.1 μm particle stream is found to vary slightly at about 130 μm for the range of flow rates under test. This indicates that 3.1 μm particles remain confined within the

DOI: 10.1021/acs.analchem.5b00752
Anal. Chem. 2015, 87, 4560−4565

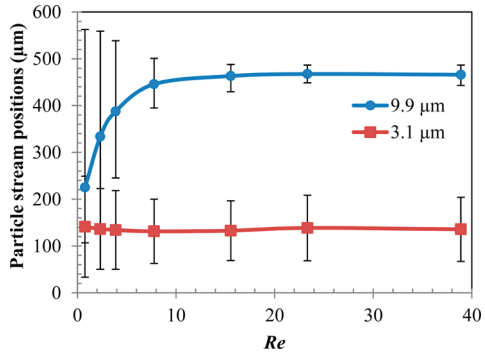

Figure 4. Comparison of the exiting positions (symbols with error bars) of 3.1 and 9.9 μm diameter particle streams vs Re at the expansion of the microchannel. The data were measured from the images in Figure 3 with reference to the top sidewall, which is indicated by the vertical arrow on the right-most image. Note that the lines are used to guide eyes only.

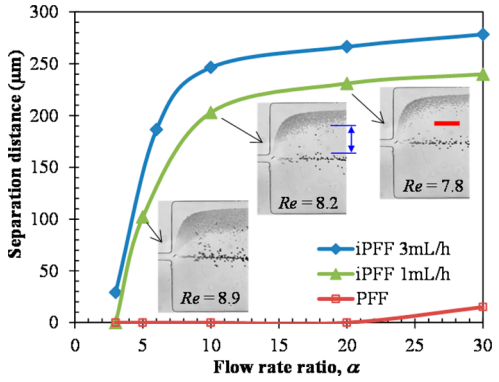

Figure 5. Comparison of the separation distances between 3.1 and 9.9 μm diameter particle streams in a 25 μm deep microchannel (i.e., AR = 2.0) via iPFF (measured directly from particle images, see, for example, the highlighted dimension on the middle inset image) and PFF (predicted from eq 6) at different flow rate ratios, α, between sheath fluid and particle mixture. The sheath flow rate in iPFF was maintained at either 1 or 3 mL/h, for the former of which three superimposed images (corresponding to α = 5, 10, and 20 from left to right) are included as insets. The scale bar represents 200 μm.

sheath flow-focused fluid, which, as noted above, is 6.3 μm wide in the 50 μm wide main branch and should become around 113 μm in the 900 μm wide expansion for laminar flows. In contrast, the inertial deflection of 9.9 μm particles is enhanced quickly with the increase of Re, which reaches the half width of the expansion at Re $\approx$ 10 and remains unvaried for higher Re values. Therefore, a complete separation of the two types of particles via iPFF is expected to be available in a large range of Re spanning from around 10 to at least 100. At the smallest flow rate with Re = 0.8, where the inertial effects are still minimal and the separation may be viewed as purely PFF, the center position of the 9.9 μm particle stream is found to locate at about 225 μm in the expansion region with a large dispersion (see Figure 4). This deflection is approximately 25% greater than the estimated value of 180 μm from the streamline analysis, which is due primarily to the neglected corner effect on particle positions.[28−31]

Effect of Flow Rate Ratio (α) between Sheath Fluid and Particle Mixture. The apparent inertia-enhanced particle displacement in Figures 3 and 4 indicates that the width of the sheath flow-focused particulate solution in the main branch of the microchannel for iPFF can be greater than $w_{p,max}$ in eq 1 for PFF. In other words, the sheath fluid to particle mixture flow rate ratio, α, can be significantly reduced, leading to a much higher particle throughput at the same sheath flow rate. Figure 5 presents the measured separation distances (see the highlighted dimension on the inset particle image) between 3.1 and 9.9 μm diameter particle streams in a 25 μm deep microchannel (i.e., AR = 2.0) when α is increased from 3 to 30. The sheath flow rate, Q_{sheath}, remains at either 1 or 3 mL/h, where for the former the calculated Re from eq 2 is found to decrease mildly from 9.9 to 7.7 in the range of α. Our 3D flow simulation in COMSOL indicates that the widths of the sheath flow-focused particulate solution are w_p = 15.5, 12.1, 8.6, 7.2, 6.3, and 5.3 μm for α = 3, 5, 10, 15, 20, and 30, respectively. The theoretically predicted particle separation distance, SD_{PFF}, in the current microchannel via PFF can thus be calculated from eq 6, which is also presented in Figure 5 for comparison with that obtained via iPFF. We see that PFF is unable to separate 3.1 and 9.9 μm particles until α increases to over 20. However, even at α = 30, only a small separation distance of 15.1 μm can be theoretically implemented in the traditional PFF.

In contrast, substantially larger separation distances of 3.1 and 9.9 μm diameter particle streams are observed in iPFF at very low values of α. As seen from Figure 5, the separation distance at α = 5 can be as high as 102 μm for Q_{sheath} = 1 mL/h. It gets further enhanced when the inertial lift plays a stronger role at Q_{sheath} = 3 mL/h, where the two particles can be separated at even α = 3 with a separation distance of around 29 μm. This indicates that the particle throughput can be enhanced by at least 1 order of magnitude in iPFF as compared to that in the traditional PFF at the same sheath flow rate. For either value of Q_{sheath}, the particle separation distance increases with the rise of α. This is mainly attributed to the reduced dispersions of both types of particles, especially significant for the smaller ones (see the inset particle images in Figure 5), as the width of the sheath flow-focused particulate solution, w_p, decreases. However, the slope of the increase in particle separation distance drops quickly for α > 10 because w_p decreases slowly in the same range of α as noted earlier. Moreover, the particle separation distance at Q_{sheath} = 3 mL/h is greater than that at Q_{sheath} = 1 mL/h for all values of α due to the weaker inertial effects in the latter circumstance.

Effect of Channel Aspect Ratio (AR). Figure 6 compares the separation of 3.1 and 9.9 μm diameter particles in 40 μm (left, AR = 1.25), 25 μm (middle, AR = 2.0), and 15 μm (right,

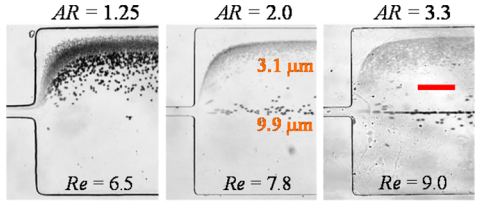

Figure 6. Superimposed images at the expansion of the main branch illustrating the effect of channel aspect ratio, AR, on the continuous separation of 3.1 and 9.9 μm diameter particles via iPFF in 40 (left), 25 (middle), and 15 μm (right) deep microchannels. The sheath flow rate was maintained at 1 mL/h and the flow rate ratio between sheath fluid and particle mixture was fixed at α = 20. The scale bar represents 200 μm.

DOI: 10.1021/acs.analchem.5b00752
Anal. Chem. 2015, 87, 4560−4565

AR = 3.3) deep microchannels. The sheath flow rate was maintained at Q_{sheath} = 1 mL/h and the flow rate ratio between sheath fluid and particle mixture was fixed at α = 20. The calculated Re (see the labeled values on the images) increases from 6.5 to 9.0 with the rise of AR. In the nearly square microchannel with AR = 1.25 (see the left image in Figure 6), the two particle streams overlap leading to an incomplete separation. This phenomenon holds true for Re ranging from 1.94 (Q_{sheath} = 0.3 mL/h) to 32.4 (Q_{sheath} = 5 mL/h; data not shown). It is probably because 9.9 μm particles have two additional equilibrium positions in a nearly square microchannel that are each approximately at 0.4 times the channel half-width from the adjacent sidewall, that is, 0.4 × ($w_{expansion}$/2) = 180 μm in the expansion.[58,59] This position is not far from the sheath flow-focused 3.1 μm particle solution (w_p = 7.5 μm in the main branch from a 3D flow simulation) that is within 135 μm from the channel sidewall in the expansion. Note that this latter value was estimated by assuming particles strictly follow streamlines, which, as noted earlier, may be influenced by the corner effect.[28−31] In contrast, the two types of particles can be separated in the rectangular microchannel with AR = 3.3 (see the right image in Figure 6), which, however, seems slightly worse than in the channel with AR = 2.0 (see the middle image). This is mainly because the 3.1 μm particle stream spans toward the channel centerline, which seems consistent with the recently observed wide band of small particles in a rectangular microchannel with AR = 4.0.[58]

CONCLUSIONS

We have demonstrated for the first time that the flow-induced inertial lift force can be utilized to significantly improve the particle separation in the traditional PFF. This inertia-enhanced PFF, which we term iPFF in short, is implemented by a simple elongation of the pinched segment in PFF, which does not rely on any external force. More importantly, iPFF can separate particles at a much higher throughput while consuming a much less amount of sheath fluid than PFF does. This proposed novel separation technique has been experimentally studied through a continuous separation of 3.1 and 9.9 μm diameter particles in rectangular microchannels with different values of AR. It is found that iPFF works the most effectively in a microchannel with AR ≈ 2.0, where the separation distance between the two types of particles quickly increases with the rise of Re when it is below 10. This happens because under the inertial effects 9.9 μm particles are directed toward the channel centerline, while 3.1 μm particles stay within the sheath-flow focused particle solution. With the further increase of Re, the particle separation distance remains nearly unvaried unless additional equilibrium positions occur for the larger particles at very high Re. It is, however, important to note that the proposed iPFF is not anticipated to work well for small particles (e.g., less than 1 μm in diameter) because the inertial lift force they experience in microfluidic devices is typically negligible.[40−42] In future work, we will study how the length of the main branch between the T-junction and expansion of the microchannel may affect the particle separation in iPFF. We will also study how the channel dimensions should scale up for separating large particles such as circulating tumor cells from blood.[62]

AUTHOR INFORMATION

Corresponding Author

*E-mail: xcxuan@clemson.edu. Tel.: 864-656-5630. Fax: 864-656-7299.

Notes

The authors declare no competing financial interest.

ACKNOWLEDGMENTS

This work was supported in part by NSF under Grant CBET-1150670 and by Clemson University through a departmental SGER (Small Grants for Exploratory Research) Grant.

REFERENCES

(1) Bhagat, A. A. S.; Bow, H.; Hou, H.; Tan, S.; Han, J.; Lim, C. *Med. Biol. Eng. Comput.* **2010**, *48*, 999−1014.
(2) Sajeesh, P.; Sen, A. K. *Microfluid. Nanofluid.* **2014**, *17*, 1−52.
(3) Tsutsui, H.; Ho, C. M. *Mech. Res. Commun.* **2009**, *36*, 92−103.
(4) Gossett, D. R.; Weaver, W. M.; Mach, A. J.; Hur, S. C.; Tse, H. T.; Lee, W.; Amini, H.; Di Carlo, D. *Anal. Bioanal. Chem.* **2010**, *397*, 3249−3267.
(5) Autebert, J.; Coudert, B.; Bidard, F.; Pierga, J.; Descroix, S.; Malaquin, L.; Viovy, J. *Methods* **2012**, *57*, 297−307.
(6) Watarai, H. *Annu. Rev. Anal. Chem.* **2013**, *6*, 353−378.
(7) Li, M.; Li, W.; Zhang, J.; Alici, G.; Wen, W. *J. Phys. D: Appl. Phys.* **2014**, *47*, 063001.
(8) Shields, C. W., IV; Reyes, C. D.; Lopez, G. P. *Lab Chip* **2015**, *15*, 1230−1249.
(9) Yamada, M.; Nakashima, M.; Seki, M. *Anal. Chem.* **2004**, *76*, 5465−5471.
(10) Maenaka, H.; Yamada, M.; Yasuda, M.; Seki, M. *Langmuir* **2008**, *24*, 4405−4410.
(11) Larsen, A. V.; Poulsen, L.; Birgens, H.; Dufva, M.; Kristensen, A. *Lab Chip* **2008**, *8*, 818−821.
(12) Cupelli, C.; Borchardt, T.; Steiner, T.; Paust, N.; Zengerle, R.; Santer, M. *Microfluid. Nanofluid.* **2013**, *14*, 551−563.
(13) Kawamata, T.; Yamada, M.; Yasuda, M.; Seki, M. *Electrophoresis* **2008**, *29*, 1423−1430.
(14) Wu, Z.; Li, A.; Hjort, K. *J. Micromech. Microeng.* **2007**, *17*, 1992−1999.
(15) Mortensen, N. A. *Anal. Chem.* **2007**, *79*, 9240−9241.
(16) Lee, K. H.; Kim, S. B.; Lee, K. S.; Sung, H. J. *Lab Chip* **2011**, *11*, 354−357.
(17) Morijiri, M.; Sunahiro, S.; Senaha, M.; Yamada, M.; Seki, M. *Microfluid. Nanofluid.* **2011**, *11*, 105−110.
(18) Lu, X.; Hsu, J. P.; Xuan, X. *Langmuir* **2015**, *31*, 620−627.
(19) Vig, A. L.; Kristensen, A. *Appl. Phys. Lett.* **2008**, *93*, 203507.
(20) Takagi, J.; Yamada, M.; Yasuda, M.; Seki, M. *Lab Chip* **2005**, *5*, 778−784.
(21) Sai, Y.; Yamada, M.; Yasuda, M.; Seki, M. *J. Chromatogr. A* **2006**, *1127*, 214−220.
(22) Zhang, X.; Cooper, J. M.; Monaghan, P. B.; Haswell, S. J. *Lab Chip* **2006**, *6*, 561−566.
(23) Andersen, K. B.; Levinsen, S.; Svendsen, W. E.; Okkels, F. *Lab Chip* **2009**, *9*, 1638−1639.
(24) Srivastav, A.; Podgorski, T.; Coupier, G. *Microfluid. Nanofluid.* **2012**, *13*, 697−701.
(25) Wu, Z.; Hjort, K.; Wicher, G.; Svenningsen, A. F. *Biomed. Microdev.* **2008**, *10*, 631−638.
(26) Jain, A.; Posner, J. D. *Anal. Chem.* **2008**, *80*, 1641−1648.
(27) Nho, H. W.; Yoon, T. H. *Lab Chip* **2013**, *13*, 773−776.
(28) Zinchenko, A. Z.; Ashley, J. F.; Davis, R. H. *Phys. Fluid.* **2012**, *24*, 043302.
(29) Bowman, C. N.; Ashley, J. F.; Davis, R. H. *AIChE J.* **2013**, *59*, 3444−3457.
(30) Shardt, O.; Mitra, S. K.; Derksen, J. J. *Chem. Eng. Sci.* **2012**, *75*, 106−119.
(31) Risbud, S. R.; Drazer, G. *Microfluid. Nanofluid.* **2014**, *17*, 1003−1009.
(32) Segre, G.; Silberberg, A. *Nature* **1961**, *189*, 209−210.
(33) Cox, R. G.; Brenner, H. *Chem. Eng. Sci.* **1968**, *23*, 147−173.
(34) Ho, B. P.; Leal, L. G. *J. Fluid Mech.* **1974**, *65*, 365−400.
(35) Leal, L. G. *Annu. Rev. Fluid Mech.* **1980**, *12*, 436−476.

DOI: 10.1021/acs.analchem.5b00752
Anal. Chem. 2015, 87, 4560−4565

(36) Schonberg, J. A.; Hinch, E. J. *J. Fluid Mech.* **1989**, *203*, 517−524.
(37) Asmolov, E. S. *J. Fluid Mech.* **1999**, *381*, 63−87.
(38) Matas, J.; Morris, J. F.; Guazzelli, E. *J. Fluid Mech.* **2004**, *515*, 171−195.
(39) Di Carlo, D.; Irimia, D.; Tompkins, R. G.; Toner, M. *Proc. Natl. Acad. Sci. U.S.A.* **2007**, *104*, 18892−18897.
(40) Di Carlo, D. *Lab Chip* **2009**, *9*, 3038−3046.
(41) Amini, H.; Lee, W.; Di Carlo, D. *Lab Chip* **2014**, *14*, 2739−2761.
(42) Martel, J. M.; Toner, M. *Annu. Rev. Biomed. Eng.* **2014**, *16*, 371−396.
(43) Nieuwstadt, H. A.; Seda, R.; Li, D. S.; Fowlkes, J. B.; Bull, J. L. *Biomed. Microdev.* **2011**, *13*, 97−105.
(44) Hur, S. C.; Henderson-MacLennan, N. K.; McCabec, E. R. B.; Di Carlo, D. *Lab Chip* **2011**, *11*, 912−920.
(45) Parichehreha, V.; Sethu, P. *Lab Chip* **2012**, *12*, 1296−1301.
(46) Hou, H.; Gan, H. Y.; Bhagat, A. A. S.; Li, L. D.; Lim, C. T.; Han, J. *Biomicrofluidics* **2012**, *6*, 024115.
(47) Zhou, J.; Kasper, S.; Giridhar, P. V.; Papautsky, I. *Biomicrofluidics* **2014**, *8*, 044112.
(48) Di Carlo, D.; Edd, J. F.; Irimia, D.; Tompkins, R. G.; Toner, M. *Anal. Chem.* **2008**, *80*, 2204−2211.
(49) Wu, L.; Guan, G.; Hou, H.; Bhagat, A. A. S.; Han, J. *Anal. Chem.* **2012**, *84*, 9324−9331.
(50) Sun, J.; Liu, C.; Li, M.; Wang, J.; Xianyu, Y.; Hu, G.; Jiang, X. *Biomicrofluidics* **2013**, *7*, 011802.
(51) Nivedita, N.; Papautsky, I. *Biomicrofluidics* **2013**, *7*, 054101.
(52) Zhang, J.; Yan, S.; Li, W.; Alicia, G.; Nguyen, N. T. *RSC Adv.* **2014**, *4*, 33149−33159.
(53) Park, J. S.; Jung, H. *Anal. Chem.* **2009**, *81*, 8280−8288.
(54) Hur, S. C.; Mach, A. J.; Di Carloa, D. *Biomicrofluidics* **2011**, *5*, 022206.
(55) Lee, M. G.; Shin, J. H.; Bae, C. Y.; Choi, S.; Park, J. K. *Anal. Chem.* **2013**, *85*, 6213−6218.
(56) Lu, X.; Patel, S.; Zhang, M.; Joo, S.; Qian, S.; Ogale, A.; Xuan, X. *Biomicrofluidics* **2014**, *8*, 021802.
(57) Zhou, J.; Papautsky, I. *Lab Chip* **2013**, *13*, 1121−1132.
(58) Liu, C.; Hu, G.; Jiang, X.; Sun, J. *Lab Chip* **2015**, *15*, 1168−1177.
(59) Di Carlo, D.; Edd, J. F.; Humphry, K. J.; Stone, H. A.; Toner, M. *Phys. Rev. Lett.* **2009**, *102*, 094503.
(60) Saffman, P. G. *J. Fluid Mech.* **1965**, *22*, 385−400.
(61) Plouffe, B. D.; Murthy, S. K. *Anal. Chem.* **2014**, *23*, 11481−11488.
(62) Zhang, J.; Li, W.; Li, M.; Alici, G.; Nguyen, N. T. *Microfluid. Nanofluid.* **2014**, *17*, 305−316.

DOI: 10.1021/acs.analchem.5b00752
Anal. Chem. 2015, 87, 4560−4565